

Received May 31, 2020, accepted June 8, 2020, date of publication June 11, 2020, date of current version June 26, 2020.

Digital Object Identifier 10.1109/ACCESS.2020.3001653

Kinematic Analysis of a Serial-Parallel Hybrid Mechanism and Its Application to a Wheel-Legged Robot

JIANYE NIU^{1,2}, HONGBO WANG^{1,3}, (Member, IEEE), ZHIWEN JIANG^{1,2}, LI CHEN^{1,2},

JIANJUN ZHANG^{1,2}, YONGFEI FENG⁴, AND SHIJIE GUO^{1,2}, (Member, IEEE)

¹State Key Laboratory of Reliability and Intelligence of Electrical Equipment, Hebei University of Technology, Tianjin 300130, China

²Hebei Key Laboratory of Robot Perception and Human-Robot Interaction, Hebei University of Technology, Tianjin 300130, China

³Parallel Robot and Mechatronic System Laboratory of Hebei Province, Yanshan University, Qinhuangdao 066004, China

⁴Faculty of Mechanical Engineering and Mechanics, Ningbo University, Ningbo 315211, China

Corresponding authors: Hongbo Wang (hongbo_w@ysu.edu.cn) and Shijie Guo (guoshijie@hebut.edu.cn)

This work was supported in part by the National Key Research and Development Program of China under Grant 2019YFB1312500 and Grant 2016YFE0128700, in part by the Project Funded by the China Postdoctoral Science Foundation under Grant 2019M660963 and Grant 2019M660964, and in part by the European Commission Marie Skłodowska-Curie SMOOTH (Smart Robots for Firefighting) Project under Grant H2020-MSCA-RISE-2016-734875.

ABSTRACT A three-DOF (degree-of-freedom) serial-parallel hybrid mechanism is proposed that consists of a 2-UPS+U component (UPS: universal-/prismatic-/spherical-joint chain and U: universal joint) and an R+RPS component (R: revolute joint and RPS: revolute-/prismatic-/spherical-joint chain). This mechanism can provide high precision and a large workspace, which indicates its applicability to wheel-legged robots. To verify our proposal, a mobility analysis showed that the mechanism simultaneously achieved three rotational movements. Then, the inverse/forward position analysis, velocity analysis, acceleration analysis, and stiffness analysis were carried out. Finally, a prototype of the mechanism was fabricated and its position error was found to be <1.8% despite the large workspace. These results demonstrate the effectiveness of our proposal and provide a new approach for designing new mechanisms for wheel-legged robots.

INDEX TERMS Serial-parallel hybrid mechanism, 2-UPS+U mechanism, R+RPS mechanism, kinematics, wheel-legged robot.

I. INTRODUCTION

Wheel-legged mobile robots (WLMRs) have attracted much attention because of their adaptability to various environments [1]. A WLMR is a hybrid system of a legged robot and a wheeled robot. A WLMR moves quickly and efficiently on wheels in flat road conditions, but can also function in complex road conditions, such as rugged and muddy roads, and pass through obstacles with legs.

WLMRs can be roughly divided into three types according to design concept. (1) A wheeled structure with a legged suspension, e.g., ANYmal and ATHLETE [2]–[13]. The wheel and the leg are generally connected in series, with the wheel set at the end of the leg. (2) A legged/wheeled alternative structure, e.g., Halluc IIx [14] and NOROS [15]. To improve the speed on flat roads, driving/passive wheels are mounted

The associate editor coordinating the review of this manuscript and approving it for publication was Tao Wang^{1,2}.

on the leg. Here, depending on road conditions, the two modes can be freely switched with a legged/wheeled conversion device. (3) A simple combination of wheeled and legged robots, e.g., Handle [16]–[18].

The majority of the above WLMRs adopt serial mechanisms, which offer advantages such as easily arranged joints, large workspaces, and simple controllability, but their low stiffness makes them less accurate in both motion and capacity. In contrast, parallel mechanisms are capable of carrying heavy loads with high motion accuracy but suffer from small workspaces, strong motion restriction caused by the other components, and control difficulties. Clearly, these advantages and disadvantages are complementary; this indicates that combining them in a hybrid mechanism design would provide the advantages of both serial and parallel mechanisms. Thus, the serial-parallel hybrid mechanism (SPM) has emerged as a choice for the innovative design of robot mechanisms.

To date, some trials have been conducted to apply SPMs to robots. Thornton [19] proposed an assembly robot, the GEC Tetrabot, which serially combines a 3-DOF wrist manipulator and a 3-DOF parallel mechanism. This design created a relatively large workspace compared to conventional parallel mechanisms. Giuseppe and Marco [20] devised a serial/parallel robot for surgical use by serially connecting a SCARA robot and a 3-DOF parallel manipulator. Cha *et al.* [21] developed a robot for road maintenance based on SPMs, which connects a 6-UPS (UPS: universal-/prismatic-/spherical-joint chain) parallel manipulator to a 3-DOF serial frame. Gao *et al.* [22] designed a quadruped walking robot based on SPMs. The leg of this robot serially includes a 3-RRR (R: rotation joint) parallel mechanism and an R joint, used as the hip and knee joints, respectively. Hou *et al.* [23] proposed a 5-DOF manipulator based on an RP-(2-RRU/1-RUU) mechanism. Peidró *et al.* [24] developed a humanoid robot with a serial/parallel hybrid structure; its leg incorporates two parallel mechanisms that are connected in series. Zhang and Gao [25] combined two parallel mechanisms in series to form a robot, obtaining a large workspace and high accuracy. Lu *et al.* [26] developed a serial-parallel hybrid manipulator with an upper 3RPS (RPS: revolute-/prismatic-/spherical-joint chain) parallel mechanism and a lower 3SPR mechanism and used it to build a hand with three fingers. Wang *et al.* [27] devised an SPM as the leg of a quadruped robot, with a four-bar parallel mechanism and five-bar mechanism in series.

The above results demonstrate that SPMs can be categorized into two types: (1) Two parallel mechanisms that are serially connected and (2) serial and parallel mechanisms that are serially connected [28]. The first type has been rarely reported, as it is difficult to construct theoretical models for analysis and control. In contrast, the second type has been broadly studied, as the parallel mechanism can achieve high position accuracy, while the serial mechanism can improve the dexterity and enlarge the workspace.

We propose an SPM [29] and apply it as a leg for a wheel-legged robot. This SPM essentially consists of a 2-UPS+U and an R, and it belongs to type (2). In [29] the workspace of the SPM was found, showing that the mechanism has a larger workspace compared with the workspace of conventional parallel mechanism. Thus, as the PM in this study is structurally similar to the previous one, it should inherently exhibit the merit of large workspace. However, the stiffness of the entire mechanism is insufficient because of the serial portion. To mitigate this problem, in this study, we improve the previous mechanism by adding an RPS chain and forming a new mechanism, namely, a (2-UPS+U)&(R+RPS). Here, using an RPS chain is capable of forming a double R-pairs connection type, which enhances the stiffness of the entire mechanism and consequently improves the motion accuracy. In addition, because the new mechanism is structurally similar to the previous mechanism, it can provide a large workspace. These features allow us to infer that our proposal

TABLE 1. Symbol of each part of the mechanism.

Parameter	Symbol	Parameter	Symbol
Length of OK	l_1	Length of B_3C_3	l_{03}
Length of KP	l_2	Length of C_3D_3	b_3
Length of OA_1	a_1	Distance of OC_1	c_1
Length of OA_2	a_2	Distance of OC_2	c_2
Length of A_1B_1	l_{01}	Distance of KD_3	c_3
Length of B_1C_1	b_1	Distance of KA_3	c_4
Length of A_2B_2	l_{02}	Range of angle α	$-5^\circ\sim40^\circ$
Length of B_2C_2	b_2	Range of angle β	$-25^\circ\sim25^\circ$
Length of A_3B_3	a_3	Range of angle γ	$-30^\circ\sim90^\circ$

would provide a good candidate mechanism for wheel-legged robots.

In this paper, the configuration of the (2-UPS+U)&(R+RPS) is first introduced, and its mobility is demonstrated. Subsequently, the kinematics are theoretically analyzed, and the results are verified through simulation. Finally, a mechanism prototype is fabricated, and its performance is experimentally evaluated to assess the feasibility of our proposal.

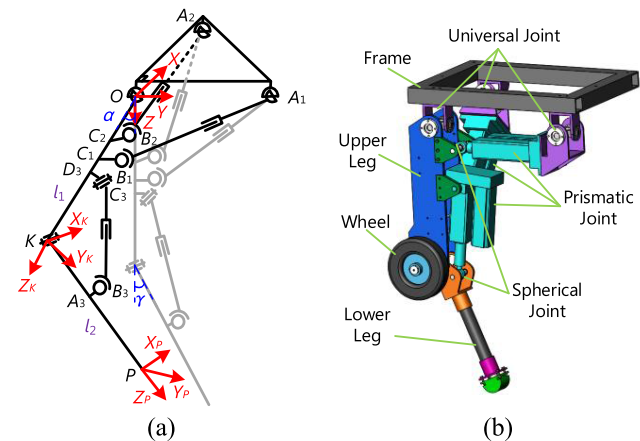


FIGURE 1. Configuration of the (2-UPS+U)&(R+RPS) mechanism. (a) The schematic, with the gray line indicating the initial posture ($\alpha = 0$, $\beta = 0$, $\gamma = -30^\circ$) and the black line indicating the arbitrary posture. (b) The 3D model.

II. CONFIGURATION AND DOF ANALYSIS

A. CONFIGURATION

Figs. 1(a) and (b) illustrate the mechanism's schematic and 3D model, respectively. An RPS kinematic chain is added between the limbs l_1 and l_2 . The P pair is an active joint, the R and S pairs are passive joints, and the rotation of l_2 is achieved with the actuator l_{03} .

To facilitate the following analysis, we have named the symbol of each part of the mechanism, as shown in Table 1.

B. DOF ANALYSIS

First, the DOF of the (2-UPS+U)&(R+RPS) mechanism is analyzed to clarify its mobility. Because the configuration

is a spatial SPM, the DOF is obtained with the modified Kutzbach-Grübler formula [30], [31]:

$$M = d(n - g - 1) + \sum_{i=1}^g f_i + v - \eta. \quad (1)$$

In the mechanism, the order d equals 6, the number of components n equals 9, the number of kinematic pairs g equals 11, and the sum of the DOFs of all the kinematic pairs $\sum f_i$ equals 20. The UPS chain's DOF is 6, and the kinematic chain does not have any constraint on the mechanism, so the 2-UPS+U does not have a redundant constraint. In the R+RPS, the analysis shows that this part has 1 DOF and 5 effective constraints, and the total number of constraints is 6 (the R pair has 5 constraints, and the RPS chain has 1 constraint), so the redundant constraint v is 1 ($6-5=1$); see the analysis below for details. In addition, there is no local DOF in the mechanism (indicating that $\eta = 0$). According to (1), the mechanism's DOF is 3.

Then, the mobility of the mechanism is analyzed based on screw theory [32], [33]. In the 2-UPS+U, the U pair between the frame and the upper limb l_1 can be equivalently treated as two revolute joints, so there are two screws: $\$1$ and $\$2$. On the other hand, in the constraint wrench of this part, obtained based on the reciprocal screw theory, there are four constraint wrenches: $\$1^r$, $\$2^r$, $\$3^r$ and $\$4^r$. Thus, the kinematic screws and constraint wrenches of the 2-UPS+U can be expressed as

$$\begin{cases} \$1 = (1\ 0\ 0; \ 0\ 0\ 0) \\ \$2 = (0\ 1\ 0; \ 0\ 0\ 0) \\ \$1 = (1\ 0\ 0; \ 0\ 0\ 0) \\ \$2 = (0\ 1\ 0; \ 0\ 0\ 0) \\ \$3 = (0\ 0\ 1; \ 0\ 0\ 0) \\ \$4 = (0\ 0\ 0; \ 0\ 0\ 1). \end{cases} \quad (2)$$

Here, the four constraint wrenches constrain three movements in the x -, y - and z -axes and the rotation in the z -axis, respectively. Thus, the 2-UPS+U retains 2 DOFs, i.e., the rotations in the x - and y -axes.

In the R+RPS, the R pair has one screw $\$1'$ and five constraint wrenches $\$1'^r$, $\$2'^r$, $\$3'^r$, $\$4'^r$ and $\$5'^r$; the kinematic screws and constraint wrenches of the R pair can be expressed as

$$\begin{cases} \$1' = (1\ 0\ 0; \ 0\ 0\ 0) \\ \$1'^r = (1\ 0\ 0; \ 0\ 0\ 0) \\ \$2'^r = (0\ 1\ 0; \ 0\ 0\ 0) \\ \$3'^r = (0\ 0\ 1; \ 0\ 0\ 0) \\ \$4'^r = (0\ 0\ 0; \ 0\ 1\ 0) \\ \$5'^r = (0\ 0\ 0; \ 0\ 0\ 1). \end{cases} \quad (3)$$

Meanwhile, the RPS chain has five screws, $\$1''$, $\$2''$, $\$3''$, $\$4''$ and $\$5''$, and one constraint wrench $\$5''^r$, as shown in Fig. 2. Thus, the kinematic screws and constraint wrenches of the

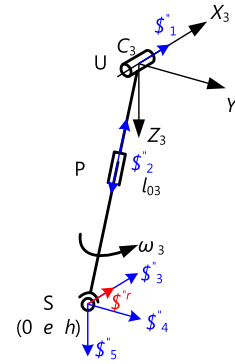


FIGURE 2. Kinematic screws and constraint wrench of the RPS chain.

RPS chain can be expressed as

$$\begin{cases} \$1'' = (1\ 0\ 0; \ 0\ 0\ 0) \\ \$2'' = (0\ 0\ 0; \ 0\ e\ h) \\ \$3'' = (1\ 0\ 0; \ 0\ h\ -e) \\ \$4'' = (0\ 1\ 0; \ -h\ 0\ 0) \\ \$5'' = (0\ 0\ 1; \ e\ 0\ 0) \\ \$5''^r = (1\ 0\ 0; \ 0\ h\ -e). \end{cases} \quad (4)$$

where $[0\ e\ h]^T$ is the position coordinate of the S pair in the $C_3 - x_3y_3z_3$ coordinate system.

By (3) and (4), we can see that $\text{rank } (\$1'^r \ \$2'^r \ \$3'^r \ \$4'^r \ \$5'^r)^T = 5$, i.e., $\$5'^r$ is linearly correlated with $\$1'^r$, $\$2'^r$, $\$3'^r$, $\$4'^r$ and $\$5'^r$, so $\$5'^r$ is a redundant constraint. Thus, the R+RPS retains 1 DOF, i.e., the rotation in the x_k -axis.

In summation, the 3 DOFs of the (2-UPS+U)&(R+RPS) mechanism are the rotations in the x -, y - and x_k -axes.

III. KINEMATIC ANALYSIS

A. POSITION ANALYSIS

1) FORWARD POSITION ANALYSIS

A forward position analysis of the (2-UPS+U)&(R+RPS) mechanism is implemented in the coordinate systems shown in Fig. 1(a). $O-xyz$ is a global coordinate system, α and β are the rotation angles in the x - and y -axes, and γ is the rotation angle in the x_k -axis in a moving coordinate system $K-x_ky_kz_k$. To clarify the position of the end point (P) in $O-xyz$, it can be calculated with the following steps:

Express the position vector of point K in $O-xyz$ as

$${}^O_K \mathbf{K} = {}^O_R \mathbf{R} \cdot l_1 = [l_1 \cos \alpha \sin \beta \ -l_1 \sin \alpha \ l_1 \cos \alpha \cos \beta]^T, \quad (5)$$

where ${}^O_R \mathbf{R} = \text{Rot}(Y, \beta)\text{Rot}(X, \alpha)$ and $l_1 = [0\ 0\ l_1]^T$ is the vector of limb l_1 .

Determine the relationship between $O-xyz$ and $K-x_ky_kz_k$ and express it with a transformation matrix

$${}^O_K T = \begin{bmatrix} {}^O_R & {}^O_K \\ 0_{1 \times 3} & 1 \end{bmatrix}. \quad (6)$$

Through the coordinate transform, the point p position in $K-x_ky_kz_k$ is obtained as

$${}^K P = {}^O_R \mathbf{R} \cdot l_2, \quad (7)$$

where ${}^K_P \mathbf{R} = \text{Rot}(X_K, \gamma)$ and $\mathbf{l}_2 = [0 \ 0 \ l_2]^T$ is the vector of limb \mathbf{l}_2 .

Determine the relationship between the moving coordinate system $P\text{-}x_p y_p z_p$ and $K\text{-}x_k y_k z_k$ by using a homogeneous transformation matrix:

$${}^P_K \mathbf{T} = \begin{bmatrix} {}^K \mathbf{R} & {}^K \mathbf{P} \\ P_{1 \times 3} & 1 \end{bmatrix}, \quad (8)$$

Multiply (6) by (8) and build the relationship between $O\text{-}xyz$ and $P\text{-}x_p y_p z_p$:

$${}^O \mathbf{T} = {}^O_K \mathbf{T} {}^K_P \mathbf{T} \quad (9)$$

Calculate the position vector of the end point P in $O\text{-}xyz$ as

$$\begin{bmatrix} p_x \\ p_y \\ p_z \end{bmatrix} = \begin{bmatrix} (l_2 \cos(\alpha + \gamma) + l_1 \cos \alpha) \sin \beta \\ -l_2 \sin(\alpha + \gamma) - l_1 \sin \alpha \\ (l_2 \cos(\alpha + \gamma) + l_1 \cos \alpha) \cos \beta \end{bmatrix}. \quad (10)$$

From (10), the relationships between the point P position (p_x, p_y, p_z) and the three rotation angles α, β and γ are obtained. Next, the relationships between α, β and γ and the lengths of the electric push rods l_{01}, l_{02} , and l_{03} need to be analyzed to determine the actuating method.

The central positions of the three U pairs in $O\text{-}xyz$ are

$${}^O \mathbf{O} = \begin{bmatrix} 0 \\ 0 \\ 0 \end{bmatrix}, \quad {}^O \mathbf{A}_1 = \begin{bmatrix} 0 \\ a_1 \\ 0 \end{bmatrix}, \quad {}^O \mathbf{A}_2 = \begin{bmatrix} a_2 \\ 0 \\ 0 \end{bmatrix}. \quad (11)$$

The central position of each point of the upper limb in $O\text{-}xyz$ are

$$\left\{ \begin{array}{l} {}^O \mathbf{B}_1 = \begin{bmatrix} 0 \\ b_1 \\ c_1 \end{bmatrix}, {}^O \mathbf{B}_2 = \begin{bmatrix} b_2 \\ 0 \\ c_2 \end{bmatrix}, {}^K \mathbf{C}_1 = \begin{bmatrix} 0 \\ 0 \\ c_1 \end{bmatrix}, \\ {}^O \mathbf{C}_2 = \begin{bmatrix} 0 \\ 0 \\ c_2 \end{bmatrix} \\ {}^O \mathbf{K} = \begin{bmatrix} 0 \\ 0 \\ l_1 \end{bmatrix}, {}^O \mathbf{C}_3 = \begin{bmatrix} 0 \\ b_3 \\ l_1 - c_3 \end{bmatrix}, {}^O \mathbf{D}_3 = \begin{bmatrix} 0 \\ 0 \\ l_1 - c_3 \end{bmatrix}. \end{array} \right. \quad (12)$$

The central position of each point of the lower limb in $K\text{-}x_k y_k z_k$ are

$${}^K \mathbf{K} = \begin{bmatrix} 0 \\ 0 \\ 0 \end{bmatrix}, \quad {}^K \mathbf{A}_3 = \begin{bmatrix} 0 \\ 0 \\ c_4 \end{bmatrix}, \quad {}^K \mathbf{B}_3 = \begin{bmatrix} 0 \\ a_3 \\ c_4 \end{bmatrix}, \quad {}^K \mathbf{P} = \begin{bmatrix} 0 \\ 0 \\ l_2 \end{bmatrix}. \quad (13)$$

Accordingly, the lengths of l_{01} and l_{02} can be determined from α and β with the following equation:

$$l_{0i} = \| {}^O \mathbf{R} {}^O \mathbf{B}_i - {}^O \mathbf{A}_i \| \quad (i = 1, 2), \quad (14)$$

where $\|\cdot\|$ represents the 2-norm of the vector.

Using (11)-(14), l_{01} and l_{02} can be expressed with geometrical parameters as (15), shown at the bottom of this page, where $s\alpha = \sin \alpha$, $c\alpha = \cos \alpha$, $s\beta = \sin \beta$, and $c\beta = \cos \beta$. (15) provides an approach to obtain the angle α and β by adjusting l_{01} and l_{02} . In particular,

$$\alpha = \arcsin\left(\frac{-B + \sqrt{B^2 - 4AC}}{2A}\right), \quad (16)$$

where

$$\begin{aligned} A &= \frac{b_1^2 + c_1^2}{b_1^2}, \\ B &= \frac{c_1(a_1^2 + b_1^2 + c_1^2 - l_{01}^2)}{a_1 b_1^2}, \end{aligned}$$

and

$$C = \frac{(a_1^2 + b_1^2 + c_1^2 - l_{01}^2)^2 - 4a_1^2 b_1^2}{4a_1^2 b_1^2}.$$

In addition,

$$\beta = \arcsin\left(\frac{-B' + \sqrt{B'^2 - 4A'C'}}{2A'}\right), \quad (17)$$

where

$$\begin{aligned} A' &= \frac{b_2^2 + c_2^2 \cos^2 \alpha}{b_2^2}, \\ B' &= -\frac{c_2 \cos \alpha (a_2^2 + b_2^2 + c_2^2 - l_{02}^2)}{a_2 b_2^2}, \end{aligned}$$

and

$$C' = \frac{(a_2^2 + b_2^2 + c_2^2 - l_{02}^2)^2 - 4a_2^2 b_2^2}{4a_2^2 b_2^2}.$$

The relationship between the rotation angle γ and the length of the electric push rod l_{03} can be obtained as (18), shown at the bottom of the next page.

Then, the expression of γ can be obtained from (17)

$$\begin{aligned} \gamma &= \arctan \frac{b_3}{c_3} + \arctan \frac{a_3}{c_4} \\ &\quad + \arccos\left(\frac{a_3^2 + b_3^2 + c_3^2 + c_4^2 - l_{03}^2}{2\sqrt{b_3^2 + c_3^2}\sqrt{a_3^2 + c_4^2}}\right) - \pi \end{aligned} \quad (19)$$

Through the adjustment of l_{01}, l_{02} and l_{03} , the designed values of α, β and γ and the consequently designed point P position are achievable with (16), (17), and (19). The above process is the forward position analysis. Next, the inverse position is analyzed to provide a basis for trajectory planning.

$$\begin{cases} l_{01} = \sqrt{(c_1 c \alpha s \beta + b_1 s \alpha s \beta)^2 + (b_1 c \alpha - c_1 s \alpha - a_1)^2 + (b_1 s \alpha c \beta + c_1 c \alpha c \beta)^2} \\ l_{02} = \sqrt{(b_2 c \beta + c_2 c \alpha s \beta - a_2)^2 + (-c_2 s \alpha)^2 + (c_2 c \alpha c \beta - b_2 s \beta)^2}, \end{cases} \quad (15)$$

2) INVERSE POSITION ANALYSIS

Through inverse position analysis, a method to adjust the l_{01} , l_{02} and l_{03} can be established to obtain the desirable position (p_x, p_y, p_z) of point P in O-xyz. First, the values of α , β and γ should be solved from the point P position. In Fig. 1(a), we draw a vertical line from point O to the ground, and the foot is denoted as O' . Then, point O to P and point O' to P are connected to construct triangles ΔOKP and $\Delta OO'P$. According to the cosine theorem, we obtain

$$\begin{cases} \alpha = \arccos\left(\frac{l_1^2 + (p_x^2 + p_y^2 + p_z^2) - l_2^2}{2l_1\sqrt{p_x^2 + p_y^2 + p_z^2}}\right) - \arctan\left(\frac{p_y}{p_z}\right) \\ \beta = \arctan\left(\frac{p_x}{p_z}\right) \\ \gamma = \arccos\left(\frac{l_1^2 + l_2^2 - (p_x^2 + p_y^2 + p_z^2)}{2l_1l_2}\right) - \pi. \end{cases} \quad (20)$$

By substituting α , β and γ obtained from (20) into (15) and (18), the lengths of three electric push rods l_{01} , l_{02} and l_{03} can be determined.

B. VELOCITY ANALYSIS

1) JACOBIAN MATRIX

The Jacobian matrix is a commonly used concept for velocity analysis, and it reflects the mapping relationship between the operating space and joint space.

In the (2-UPS+U)&(R+RPS) mechanism, the velocity in the operating space is referred to as the linear velocity of point P, and the velocity in the joint space includes two rotational angular velocities $\dot{\alpha}$ and $\dot{\beta}$ of the upper limb's U-pair and the rotational angular velocity $\dot{\gamma}$ of joint K. Therefore, the Jacobian matrix of the mechanism is the mapping function between the angular velocities $\dot{\alpha}$, $\dot{\beta}$ and $\dot{\gamma}$ and the linear velocity of point P.

By acquiring the partial derivatives of p_x , p_y and p_z alternately by α , β and γ , whose relationships are given in (10), we obtain

$$\begin{cases} J_{11} = \frac{\partial p_x}{\partial \alpha} = -\sin\beta(l_2 \sin(\alpha + \gamma) + l_1 \sin\alpha) \\ J_{12} = \frac{\partial p_x}{\partial \beta} = \cos\beta(l_2 \cos(\alpha + \gamma) + l_1 \cos\alpha) \\ J_{13} = \frac{\partial p_x}{\partial \gamma} = -l_2 \sin(\alpha + \gamma) \sin\beta, \end{cases} \quad (21)$$

$$\begin{cases} J_{21} = \frac{\partial p_y}{\partial \alpha} = -l_2 \cos(\alpha + \gamma) - l_1 \cos\alpha \\ J_{22} = \frac{\partial p_y}{\partial \beta} = 0 \\ J_{23} = \frac{\partial p_y}{\partial \gamma} = -l_2 \cos(\alpha + \gamma), \end{cases} \quad (22)$$

$$\begin{cases} J_{31} = \frac{\partial p_z}{\partial \alpha} = -\cos\beta(l_2 \sin(\alpha + \gamma) + l_1 \sin\alpha) \\ J_{32} = \frac{\partial p_z}{\partial \beta} = -\sin\beta(l_2 \cos(\alpha + \gamma) + l_1 \cos\alpha) \\ J_{33} = \frac{\partial p_z}{\partial \gamma} = -l_2 \sin(\alpha + \gamma) \cos\beta, \end{cases} \quad (23)$$

After transforming (21), (22), and (23) into matrix form, we obtain

$$\begin{bmatrix} v_x \\ v_y \\ v_z \end{bmatrix} = J_{va} \begin{bmatrix} \dot{\alpha} \\ \dot{\beta} \\ \dot{\gamma} \end{bmatrix} = \begin{bmatrix} J_{11} & J_{12} & J_{13} \\ J_{21} & J_{22} & J_{23} \\ J_{31} & J_{32} & J_{33} \end{bmatrix} \begin{bmatrix} \dot{\alpha} \\ \dot{\beta} \\ \dot{\gamma} \end{bmatrix}, \quad (24)$$

where $J_{va} \in \mathbb{R}^{3 \times 3}$ is the Jacobian matrix of the (2-UPS+U)&(R+RPS) mechanism. Further, since the changes in α , β and γ are caused by l_{01} , l_{02} , and l_{03} , the actual inputs are the variation in the lengths of the three electric push rods. Therefore, the generalized Jacobian matrix between the input velocities \dot{l}_{01} , \dot{l}_{02} and \dot{l}_{03} and the linear velocity of point P can be constructed.

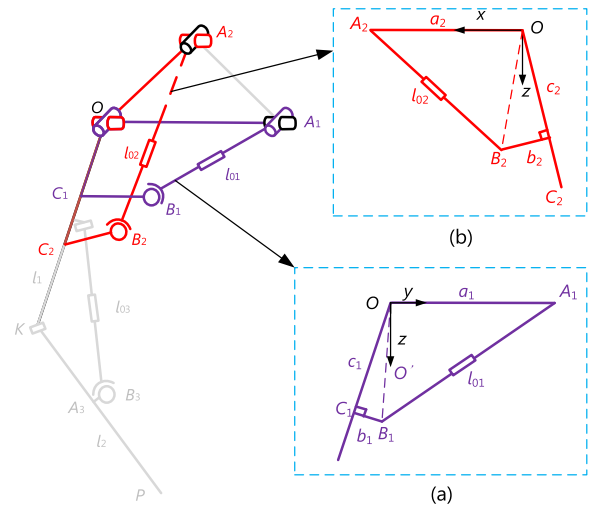


FIGURE 3. Diagram of the mechanism's Xoz and Yoz plane. (a) Yoz plane and (b) Xoz plane.

Fig. 3(a) shows that, in the quadrilateral $OA_1B_1C_1$, $OC_1 \perp B_1C_1$, OA_1 , OC_1 and B_1C_1 are fixed values, and A_1B_1 represents the length of electric push rod, l_{01} . From the geometric relationship, $\angle O'OC_1$ is the forward rotational angle α of the mechanism, so we obtain

$$\alpha = \arctan \frac{b_1}{c_1} + \arccos \left(\frac{a_1^2 + c_1^2 + b_1^2 - l_{01}^2}{2a_1\sqrt{c_1^2 + b_1^2}} \right) - \frac{\pi}{2}, \quad (25)$$

$$l_{03} = \sqrt{c_3^2 + b_3^2 + c_4^2 + a_3^2 - 2\sqrt{c_3^2 + b_3^2}\sqrt{c_4^2 + a_3^2} \cdot \cos(\pi + \gamma - \arctan \frac{b_3}{c_3} - \arctan \frac{a_3}{c_4})} \quad (18)$$

By calculating the derivatives of α and l_{01} in the time domain, we obtain

$$\dot{\alpha} = \frac{l_{01}\dot{l}_{01}}{a_1\sqrt{1 - \left(\frac{a_1^2 + c_1^2 + b_1^2 - l_{01}^2}{2a_1\sqrt{c_1^2 + b_1^2}}\right)^2}\sqrt{c_1^2 + b_1^2}}. \quad (26)$$

Similarly, the quadrilateral $OA_2B_2C_2$ shown in Fig. 3(b) demonstrates that

$$\beta = (\arctan \frac{b_2}{c_2} + \arccos \left(\frac{a_2^2 + c_2^2 + b_2^2 - l_{02}^2}{2a_2\sqrt{c_2^2 + b_2^2}} \right)) \cdot \cos \alpha - \frac{\pi}{2}, \quad (27)$$

By timely deriving β and l_{02} , we obtain

$$\begin{aligned} \dot{\beta} = & - \left[\arctan \frac{b_2}{c_2} + \arccos \left(\frac{a_2^2 + c_2^2 + b_2^2 - l_{02}^2}{2a_2\sqrt{c_2^2 + b_2^2}} \right) \right] \\ & \cdot \sin \alpha \cdot \dot{\alpha} \\ & + \cos \alpha \cdot \frac{l_{02}}{a_2\sqrt{1 - \left(\frac{a_2^2 + c_2^2 + b_2^2 - l_{02}^2}{2a_2\sqrt{c_2^2 + b_2^2}}\right)^2}\sqrt{c_2^2 + b_2^2}} \cdot \dot{l}_{02}, \end{aligned} \quad (28)$$

Similarly, by deriving γ and l_{03} in the time domain, we obtain

$$\dot{\gamma} = \frac{2l_{03}\dot{l}_{03}}{\sqrt{4(a_3^2 + c_3^2)(b_3^2 + c_3^2) - (a_3^2 + c_3^2 + b_3^2 + c_3^2 - l_{03}^2)^2}}, \quad (29)$$

Through the above analysis, the transfer function $J_{al} \in \mathbb{R}^{3 \times 3}$ between the angular velocities $\dot{\alpha}$, $\dot{\beta}$ and $\dot{\gamma}$ and the linear velocities l_{01} , l_{02} and l_{03} of the three electric push rods are

$$\begin{bmatrix} \dot{\alpha} \\ \dot{\beta} \\ \dot{\gamma} \end{bmatrix} = J_{al} \begin{bmatrix} \dot{l}_{01} \\ \dot{l}_{02} \\ \dot{l}_{03} \end{bmatrix} = \begin{bmatrix} J'_{11} 00 \\ J'_{21} J'_{22} 0 \\ 00 J'_{33} \end{bmatrix} \begin{bmatrix} \dot{l}_{01} \\ \dot{l}_{02} \\ \dot{l}_{03} \end{bmatrix}. \quad (30)$$

where

$$\begin{aligned} J'_{11} &= \frac{l_{01}}{a_1\sqrt{1 - \left(\frac{a_1^2 + c_1^2 + b_1^2 - l_{01}^2}{2a_1\sqrt{c_1^2 + b_1^2}}\right)^2}\sqrt{c_1^2 + b_1^2}}, \\ J'_{21} &= - \left[\arctan \frac{b_2}{c_2} + \arccos \left(\frac{a_2^2 + c_2^2 + b_2^2 - l_{02}^2}{2a_2\sqrt{c_2^2 + b_2^2}} \right) \right] \\ &\cdot \frac{l_{01} \cdot \sin \alpha}{a_1\sqrt{1 - \left(\frac{a_1^2 + c_1^2 + b_1^2 - l_{01}^2}{2a_1\sqrt{c_1^2 + b_1^2}}\right)^2}\sqrt{c_1^2 + b_1^2}}, \\ J'_{22} &= \frac{l_{02} \cdot \cos \alpha}{a_2\sqrt{1 - \left(\frac{a_2^2 + c_2^2 + b_2^2 - l_{02}^2}{2a_2\sqrt{c_2^2 + b_2^2}}\right)^2}\sqrt{c_2^2 + b_2^2}}, \end{aligned}$$

and

$$J'_{33} = \frac{l_{03}}{\sqrt{1 - \frac{(a_3^2 + c_3^2 + b_3^2 + c_3^2 - l_{03}^2)^2}{4(a_3^2 + c_3^2)(b_3^2 + c_3^2)}}\sqrt{(a_3^2 + c_3^2)(b_3^2 + c_3^2)}}.$$

Therefore, the Jacobian matrix between the point P velocity and the linear velocities of three electric push rods can be obtained as

$$J_{vl} = J_{va} J_{al}, \quad (31)$$

where $J_{vl} \in \mathbb{R}^{3 \times 3}$.

2) CENTROID VELOCITY OF EACH COMPONENT

Once the Jacobian matrix is obtained, we can analyze the centroid velocity of each component of the mechanism.

First, we analyze the centroid velocity of the limb l_1 . Since the limb l_1 , incorporates multiple parts and is unevenly distributed, the centroid does not locate at the geometrical center. Here, we define the centroid's initial position as l_{c1} in the $O\text{-}xyz$. The centroid velocity includes linear and angular velocities, where the angular velocity is the sum of angular velocities $\dot{\alpha}$ and $\dot{\beta}$. Thus,

$$\begin{aligned} \omega_{c1} &= \omega_\alpha + \omega_\beta + \omega_\gamma = r_\alpha \cdot \dot{\alpha} + r_\beta \cdot \dot{\beta} + \mathbf{0} \cdot \dot{\gamma} \\ &= \begin{bmatrix} \cos \beta 00 \\ 010 \\ -\sin \beta 00 \end{bmatrix} \begin{bmatrix} \dot{\alpha} \\ \dot{\beta} \\ \dot{\gamma} \end{bmatrix}, \end{aligned} \quad (32)$$

Here, $r_\alpha = \text{Rot}(Y, \beta)[0 \ 1 \ 0]^T = [\cos \beta \ 0 \ -\sin \beta]^T$ and $r_\beta = [010]^T$ are the directional vectors of the two joint angles, respectively.

Substituting (30) into (32), we obtain

$$\omega_{c1} = \begin{bmatrix} \cos \beta 00 \\ 010 \\ -\sin \beta 00 \end{bmatrix} J_{al} \begin{bmatrix} \dot{l}_{01} \\ \dot{l}_{02} \\ \dot{l}_{03} \end{bmatrix}. \quad (33)$$

Since the angular velocities of all the points on l_1 are the same, (33) is applicable to the other points on l_1 .

Based on the influence coefficient method, the linear velocity of l_1 can be obtained as

$$\begin{aligned} v_{c1} &= [r_\alpha \times {}^O\mathbf{P}_{c1} \quad r_\beta \times {}^O\mathbf{P}_{c1} \quad 0] \begin{bmatrix} \dot{\alpha} \\ \dot{\beta} \\ \dot{\gamma} \end{bmatrix} \\ &= \omega_{c1} \times {}^O\mathbf{P}_{c1} = -{}^O\mathbf{P}_{c1} \times \omega_{c1} = -S({}^O\mathbf{P}_{c1}) \cdot \omega_{c1}, \end{aligned} \quad (34)$$

where ${}^O\mathbf{P}_{c1} (= {}_K^O\mathbf{R} l_{c1})$ is the position vector of the centroid of l_1 and $S()$ represents the calculation of the skew-symmetric matrix of a vector.

Second, we analyze the centroid velocity of the limb l_2 . Here, we define the centroid's initial position as l_{c2} in the $K\text{-}x_ky_kz_k$. Through matrix transformation, the angular velocity of the centroid of l_2 is

$$\begin{aligned} \omega_{c2} &= \omega_\alpha + \omega_\beta + \omega_\gamma = r_\alpha \cdot \dot{\alpha} + r_\beta \cdot \dot{\beta} + r_\gamma \cdot \dot{\gamma} \\ &= \begin{bmatrix} \cos \beta 0 \cos \beta \\ 010 \\ -\sin \beta 0 - \sin \beta \end{bmatrix} \begin{bmatrix} \dot{\alpha} \\ \dot{\beta} \\ \dot{\gamma} \end{bmatrix}, \end{aligned} \quad (35)$$

where $r_\gamma = {}_K^O\mathbf{R} \cdot [1 \ 0 \ 0]^T = [\cos \beta \ 0 \ -\sin \beta]^T$.

The linear velocity of l_2 can be obtained as

$$\mathbf{v}_{c2} = [\mathbf{r}_\alpha \times {}^O\mathbf{P}_{c2} \quad \mathbf{r}_\beta \times {}^O\mathbf{P}_{c2} \quad \mathbf{r}_\gamma \times {}_K^O\mathbf{P}_{c2}] \begin{bmatrix} \dot{\alpha} \\ \dot{\beta} \\ \dot{\gamma} \end{bmatrix}, \quad (36)$$

where ${}^O\mathbf{P}_{c2} (= {}_K^O\mathbf{R} \cdot \mathbf{K} + {}_P^K\mathbf{R} \cdot l_{c2})$ is the position of the centroid of l_2 , \mathbf{K} is the initial position of K - $x_ky_kz_k$ in O -xyz, and ${}_K^O\mathbf{P}_{c2} (= {}_K^O\mathbf{R} \cdot {}_P^K\mathbf{R} \cdot l_{c2})$ is the position of l_2 in O -xyz.

Substituting (30) into (36), we obtain

$$\mathbf{v}_{c2} = [\mathbf{r}_\alpha \times {}^O\mathbf{P}_{c2} \quad \mathbf{r}_\beta \times {}^O\mathbf{P}_{c2} \quad \mathbf{r}_\gamma \times {}_K^O\mathbf{P}_{c2}] \mathbf{J}_{al} \begin{bmatrix} \dot{l}_{01} \\ \dot{l}_{02} \\ \dot{l}_{03} \end{bmatrix}. \quad (37)$$

Third, we analyze the centroid velocity of three kinetic limbs, i.e., two UPS chains and one RPS chain, because their large weights can affect the dynamic properties.

In the (2-UPS+U)&(R+RPS) mechanism, the S pairs of the two UPS chains are connected to the limb l_1 , so their central points $B_i(i = 1, 2)$ of the S pairs have the same velocities, equal to that of l_1 :

$$\boldsymbol{\omega}_{B_i} = \boldsymbol{\omega}_{c1} = \begin{bmatrix} \dot{\alpha} \\ \dot{\beta} \end{bmatrix} \quad (i = 1, 2), \quad (38)$$

The linear velocity of $B_i(i = 1, 2)$ is expressed as

$$\mathbf{v}_{B_i} = [\mathbf{r}_\alpha \times \mathbf{l}_{Bi} \mathbf{r}_\beta \times \mathbf{l}_{Bi}] \begin{bmatrix} \dot{\alpha} \\ \dot{\beta} \end{bmatrix}, \quad (39)$$

where \mathbf{l}_{Bi} are the positions of the central points $B_i(i = 1, 2)$ of the S pairs.

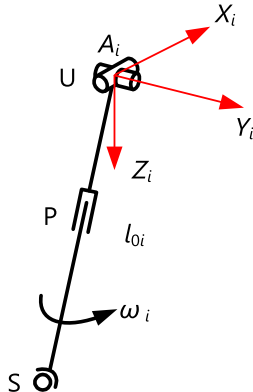


FIGURE 4. Schematic of the UPS chain. Two coordinate systems are established at points A_1 and A_2 .

Ref. [34] reported that the velocity of the UPS chain depends on that of its U pair. Therefore, we establish two local coordinate systems, i.e., $A_i - x_iy_iz_i(i = 1, 2)$ at the central point A_i of the U pairs shown in Fig. 4. Since the three U pairs are in the same direction, the $A_i-x_iy_iz_i$ are parallel to the O -xyz. Meanwhile, the rotation direction of α_i and β_i are the same as that of the U pair of l_1 . Thus,

$$\begin{bmatrix} \mathbf{v}'_{B_i} \\ \boldsymbol{\omega}'_{B_i} \end{bmatrix} = [\mathbf{r}_{\alpha i} \times \mathbf{l}_{0i} \mathbf{r}_{\beta i} \times \mathbf{l}_{0i}] \begin{bmatrix} \dot{\alpha}_i \\ \dot{\beta}_i \end{bmatrix}, \quad (40)$$

where \mathbf{l}_{0i} are the positions of the central points $B_i(i = 1, 2)$ of the S pairs in $A_i - x_iy_iz_i$, $\dot{\alpha}_i$ and $\dot{\beta}_i$ are the angular velocities of the U pair, and $\mathbf{r}_{\alpha i}$ and $\mathbf{r}_{\beta i}$ are the directional vectors of the two joint angles α_i and β_i , respectively.

Combining (38), (39) and (40), we obtain

$$\begin{bmatrix} \dot{\alpha}_i \\ \dot{\beta}_i \end{bmatrix} = G_i \begin{bmatrix} \dot{\alpha} \\ \dot{\beta} \end{bmatrix}, \quad (41)$$

where

$$G_i = \left[\frac{\mathbf{r}_{\alpha i} \times \mathbf{l}_{0i} \mathbf{r}_{\beta i} \times \mathbf{l}_{0i}}{\mathbf{r}_{\alpha i} \mathbf{r}_{\beta i}} \right]^{-1} \left[\frac{\mathbf{r}_\alpha \times \mathbf{l}_{Bi} \mathbf{r}_\beta \times \mathbf{l}_{Bi}}{\mathbf{r}_\alpha \mathbf{r}_\beta} \right] \quad (i = 1, 2). \quad (42)$$

In $A_i - x_iy_iz_i$, the velocities of the centroids of the UPS chains can be obtained as

$$\begin{bmatrix} \mathbf{v}_{c0i} \\ \boldsymbol{\omega}_{c0i} \end{bmatrix} = \left[\frac{\mathbf{r}_\alpha \times \mathbf{l}_{c0i} \mathbf{r}_\beta \times \mathbf{l}_{c0i}}{\mathbf{r}_{\alpha i} \mathbf{r}_{\beta i}} \right] \begin{bmatrix} \dot{\alpha}_i \\ \dot{\beta}_i \end{bmatrix}, \quad (43)$$

where \mathbf{l}_{c0i} are the positions of the UPS chains' centroids in $A_i - x_iy_iz_i$.

Substituting (41) into (43), the centroid velocities of the UPS chains are

$$\begin{bmatrix} \mathbf{v}_{c0i} \\ \boldsymbol{\omega}_{c0i} \end{bmatrix} = \left[\frac{\mathbf{r}_\alpha \times \mathbf{l}_{c0i} \mathbf{r}_\beta \times \mathbf{l}_{c0i}}{\mathbf{r}_{\alpha i} \mathbf{r}_{\beta i}} \right] G_i \begin{bmatrix} \dot{\alpha} \\ \dot{\beta} \end{bmatrix}. \quad (44)$$

Here, since we initially rotate l_1 by an angle α in the x -axis and then rotate by an angle β in the y -axis, some of the components in (44) can be defined as

$$\begin{cases} \mathbf{r}_{\alpha 1} = \mathbf{r}_\alpha = \begin{bmatrix} \cos \beta \\ 0 \\ -\sin \beta \end{bmatrix}, \mathbf{r}_{\beta 1} = \mathbf{r}_\beta = \begin{bmatrix} 0 \\ 1 \\ 0 \end{bmatrix} \\ \mathbf{r}_{\alpha 2} = \begin{bmatrix} \cos \beta_2 \\ 0 \\ -\sin \beta_2 \end{bmatrix}, \mathbf{r}_{\beta 1} = \mathbf{r}_\beta = \begin{bmatrix} 0 \\ 1 \\ 0 \end{bmatrix} \\ \alpha_1 = \frac{\pi}{2} - \arccos \left(\frac{a_1^2 + l_{01}^2 - (b_1^2 + c_1^2)}{2a_1l_{01}} \right), \beta_1 = \beta \\ \alpha_2 = \alpha, \beta_2 = \frac{\pi}{2} - \arccos \left(\frac{a_2^2 + l_{02}^2 - (b_2^2 + c_2^2)}{2a_2l_{02}} \right) \cdot \cos \alpha \end{cases} \quad (45)$$

Finally, the centroid velocity of the RPS chain is analyzed. The velocity of this RPS chain relies on the velocity of the R pair. Since the R pair is connected with l_1 , the angular velocity of the center point of the R pair is the same as limb l_1 . The angular velocity of the R pair in O -xyz is

$$\boldsymbol{\omega}_{c3} = \boldsymbol{\omega}_{c1} = \begin{bmatrix} \dot{\alpha} \\ \dot{\beta} \end{bmatrix}. \quad (46)$$

In O -xyz, the angular velocity of the RPS chain's centroid can be obtained as

$$\boldsymbol{\omega}_{c03} = \boldsymbol{\omega}_{c3} + \dot{\alpha}_3 = [\mathbf{r}_\alpha \mathbf{r}_\beta \mathbf{r}_{\alpha 3}] \begin{bmatrix} \dot{\alpha} \\ \dot{\beta} \\ \dot{\alpha}_3 \end{bmatrix}, \quad (47)$$

where α_3 is a function of the length of the RPS chain and can be obtained as

$$\begin{aligned} \alpha_3 &= \arctan \frac{KD_3}{C_3 D_3} \\ &+ \arccos\left(\frac{KD_3^2 + C_3 D_3^2 + l_{03}^2 - (KA_3^2 + A_3 B_3^2)}{2l_{03}\sqrt{KD_3^2 + C_3 D_3^2}}\right) - \frac{\pi}{2} \end{aligned} \quad (48)$$

By deriving α_3 and l_{03} , in the time domain, we obtain

$$\dot{\alpha}_3 = -\frac{a_3^2 - b_3^2 - c_3^2 + c_4^2 + l_{03}^2}{2l_{03}^2 \sqrt{1 - \frac{(b_3^2 + c_3^2 + l_{03}^2 - a_3^2 - c_4^2)^2}{4l_{03}^2(b_3^2 + c_3^2)}}} \cdot l_{03}. \quad (49)$$

The linear velocity of the RPS chain's centroid is

$$\mathbf{v}_{c_{03}} = [\mathbf{r}_\alpha \times {}^0\mathbf{P}_{c_{03}} \mathbf{r}_\beta \times {}^0\mathbf{P}_{c_{03}} \mathbf{r}_{\alpha 3} \times \mathbf{l}_{c_{03}}] \begin{bmatrix} \dot{\alpha} \\ \dot{\beta} \\ \dot{\gamma} \end{bmatrix}, \quad (50)$$

where ${}^0\mathbf{P}_{c_{03}}$ is the position of the RPS chain's centroid in $O\text{-}xyz$, and $\mathbf{l}_{c_{03}}$ is the position of the UPS chain's centroid in $C_3\text{-}x_3y_3z_3$ shown in Fig. 2.

C. ACCELERATION ANALYSIS

After obtaining the Jacobian matrix, we analyze the point P acceleration by partially differentiating (24) in the time domain and obtain the following equation:

$$\begin{bmatrix} a_x \\ a_y \\ a_z \end{bmatrix} = \mathbf{J}_{va} \begin{bmatrix} \ddot{\alpha} \\ \ddot{\beta} \\ \ddot{\gamma} \end{bmatrix} + [\dot{\alpha}\dot{\beta}\dot{\gamma}] \mathbf{H} \begin{bmatrix} \dot{\alpha} \\ \dot{\beta} \\ \dot{\gamma} \end{bmatrix}, \quad (51)$$

where $\mathbf{H} = [\mathbf{H}_{Px} \mathbf{H}_{Py} \mathbf{H}_{Pz}]^T$ is the Hessian matrix, which is obtained by partially differentiating each component in Jacobian matrix \mathbf{J}_{va} by α , β and γ alternately:

$$\mathbf{H}_{pj} = \begin{bmatrix} \frac{\partial^2 p_j}{\partial \alpha \cdot \partial \alpha} & \frac{\partial^2 p_j}{\partial \alpha \cdot \partial \beta} & \frac{\partial^2 p_j}{\partial \alpha \cdot \partial \gamma} \\ \frac{\partial^2 p_j}{\partial \beta \cdot \partial \alpha} & \frac{\partial^2 p_j}{\partial \beta \cdot \partial \beta} & \frac{\partial^2 p_j}{\partial \beta \cdot \partial \gamma} \\ \frac{\partial^2 p_j}{\partial \gamma \cdot \partial \alpha} & \frac{\partial^2 p_j}{\partial \gamma \cdot \partial \beta} & \frac{\partial^2 p_j}{\partial \gamma \cdot \partial \gamma} \end{bmatrix} \quad (j = x, y, z) \quad (52)$$

Similarly, the relationship between the angular acceleration of each joint and the acceleration of each electric push rod is that

$$\begin{bmatrix} \ddot{\alpha} \\ \ddot{\beta} \\ \ddot{\gamma} \end{bmatrix} = \mathbf{J}_{al} \begin{bmatrix} \ddot{l}_{01} \\ \ddot{l}_{02} \\ \ddot{l}_{03} \end{bmatrix} + [\dot{l}_{01}\dot{l}_{02}\dot{l}_{03}] \mathbf{H}' \begin{bmatrix} \dot{l}_{01} \\ \dot{l}_{02} \\ \dot{l}_{03} \end{bmatrix}, \quad (53)$$

where $\mathbf{H}' = [\mathbf{H}_\alpha \mathbf{H}_\beta \mathbf{H}_\gamma]^T$ is the Hessian matrix, obtained by partially differentiating each component in Jacobian matrix \mathbf{J}_{al} by l_{01} , l_{02} and l_{03} alternately. The results are as follows:

$$\mathbf{H}_k = \begin{bmatrix} \frac{\partial^2 k}{\partial l_{01} \cdot \partial l_{01}} & \frac{\partial^2 k}{\partial l_{01} \cdot \partial l_{02}} & \frac{\partial^2 k}{\partial l_{01} \cdot \partial l_{03}} \\ \frac{\partial^2 k}{\partial l_{02} \cdot \partial l_{01}} & \frac{\partial^2 k}{\partial l_{02} \cdot \partial l_{02}} & \frac{\partial^2 k}{\partial l_{02} \cdot \partial l_{03}} \\ \frac{\partial^2 k}{\partial l_{03} \cdot \partial l_{01}} & \frac{\partial^2 k}{\partial l_{03} \cdot \partial l_{02}} & \frac{\partial^2 k}{\partial l_{03} \cdot \partial l_{03}} \end{bmatrix} \quad (k = \alpha, \beta, \gamma) \quad (54)$$

D. INVERSE VELOCITY AND INVERSE ACCELERATION ANALYSIS

1) INVERSE VELOCITY ANALYSIS

When the velocity $[v_x v_y v_z]^T$ of point P is known, the speed $[\dot{l}_{01} \dot{l}_{02} \dot{l}_{03}]^T$ of three electric push rods can be calculated as

$$\begin{bmatrix} \dot{l}_{01} \\ \dot{l}_{02} \\ \dot{l}_{03} \end{bmatrix} = \mathbf{J}_{lv} \begin{bmatrix} v_x \\ v_y \\ v_z \end{bmatrix} = \mathbf{J}_{vl}^{-1} \begin{bmatrix} v_x \\ v_y \\ v_z \end{bmatrix} = \mathbf{J}_{al}^{-1} \mathbf{J}_{va}^{-1} \begin{bmatrix} v_x \\ v_y \\ v_z \end{bmatrix} \quad (55)$$

where $\mathbf{J}_{lv} (= \mathbf{J}_{al}^{-1} \mathbf{J}_{va}^{-1})$ is the inverse Jacobian matrix.

2) INVERSE ACCELERATION ANALYSIS

When the acceleration of the endpoint is known, there are two steps used to solve the acceleration of the three electric push rods. The first step determines the relationships between the velocities and accelerations of each joint and those of point P, and the second step determines the relationships between the joints and the electric push rods.

First, by differentiating (20), we obtain

$$\begin{bmatrix} \dot{\alpha} \\ \dot{\beta} \\ \dot{\gamma} \end{bmatrix} = \mathbf{J}_{av} \begin{bmatrix} v_x \\ v_y \\ v_z \end{bmatrix} = \begin{bmatrix} \frac{\partial \alpha}{\partial p_x} & \frac{\partial \alpha}{\partial p_y} & \frac{\partial \alpha}{\partial p_z} \\ \frac{\partial \beta}{\partial p_x} & \frac{\partial \beta}{\partial p_y} & \frac{\partial \beta}{\partial p_z} \\ \frac{\partial \gamma}{\partial p_x} & \frac{\partial \gamma}{\partial p_y} & \frac{\partial \gamma}{\partial p_z} \end{bmatrix} \begin{bmatrix} v_x \\ v_y \\ v_z \end{bmatrix}, \quad (56)$$

where $\mathbf{J}_{av} \in \mathbf{R}^{3 \times 3}$ is the matrix showing the relationships between the joint velocities and the point P velocity.

Through a partial derivation of (56), we obtain

$$\begin{bmatrix} \ddot{\alpha} \\ \ddot{\beta} \\ \ddot{\gamma} \end{bmatrix} = \mathbf{J}_{av} \begin{bmatrix} a_x \\ a_y \\ a_z \end{bmatrix} + [v_x v_y v_z] \mathbf{H}_{av} \begin{bmatrix} v_x \\ v_y \\ v_z \end{bmatrix}, \quad (57)$$

where $\mathbf{H}_{av} = [\mathbf{H}'_\alpha \mathbf{H}'_\beta \mathbf{H}'_\gamma]^T$ is the Hessian matrix obtained by partially differentiating each component in Jacobian matrix \mathbf{J}_{av} by p_x , p_y and p_z alternatively:

$$\mathbf{H}'_k = \begin{bmatrix} \frac{\partial^2 k}{\partial p_x \cdot \partial p_x} & \frac{\partial^2 k}{\partial p_x \cdot \partial p_y} & \frac{\partial^2 k}{\partial p_x \cdot \partial p_z} \\ \frac{\partial^2 k}{\partial p_y \cdot \partial p_x} & \frac{\partial^2 k}{\partial p_y \cdot \partial p_y} & \frac{\partial^2 k}{\partial p_y \cdot \partial p_z} \\ \frac{\partial^2 k}{\partial p_z \cdot \partial p_x} & \frac{\partial^2 k}{\partial p_z \cdot \partial p_y} & \frac{\partial^2 k}{\partial p_z \cdot \partial p_z} \end{bmatrix} \quad (k = \alpha, \beta, \gamma). \quad (58)$$

Then, by differentiating (15) and (18), we obtain

$$\begin{bmatrix} \dot{l}_{01} \\ \dot{l}_{02} \\ \dot{l}_{03} \end{bmatrix} = \mathbf{J}_{la} \begin{bmatrix} \dot{\alpha} \\ \dot{\beta} \\ \dot{\gamma} \end{bmatrix} = \begin{bmatrix} \frac{\partial l_{01}}{\partial \alpha} & \frac{\partial l_{01}}{\partial \beta} & \frac{\partial l_{01}}{\partial \gamma} \\ \frac{\partial l_{02}}{\partial \alpha} & \frac{\partial l_{02}}{\partial \beta} & \frac{\partial l_{02}}{\partial \gamma} \\ \frac{\partial l_{03}}{\partial \alpha} & \frac{\partial l_{03}}{\partial \beta} & \frac{\partial l_{03}}{\partial \gamma} \end{bmatrix} \begin{bmatrix} \dot{\alpha} \\ \dot{\beta} \\ \dot{\gamma} \end{bmatrix}, \quad (59)$$

where $\mathbf{J}_{la} \in \mathbf{R}^{3 \times 3}$ is the matrix indicating the relationships between the joint velocities and the electric push rod velocities.

By implementing a partial derivation of (59), we obtain

$$\begin{bmatrix} \ddot{l}_{01} \\ \ddot{l}_{02} \\ \ddot{l}_{03} \end{bmatrix} = \mathbf{J}_{la} \begin{bmatrix} \ddot{\alpha} \\ \ddot{\beta} \\ \ddot{\gamma} \end{bmatrix} + [\dot{\alpha}\dot{\beta}\dot{\gamma}] \mathbf{H}_{la} \begin{bmatrix} \dot{\alpha} \\ \dot{\beta} \\ \dot{\gamma} \end{bmatrix}, \quad (60)$$

where $\mathbf{H}_{la} = [\mathbf{H}_{l_{01}} \mathbf{H}_{l_{02}} \mathbf{H}_{l_{03}}]^T$ is the Hessian matrix, obtained by partially differentiating each component in Jacobian matrix \mathbf{J}_{la} by α , β and γ alternatively:

$$\mathbf{H}_m = \begin{bmatrix} \frac{\partial^2 m}{\partial \alpha \cdot \partial \alpha} & \frac{\partial^2 m}{\partial \alpha \cdot \partial \beta} & \frac{\partial^2 m}{\partial \alpha \cdot \partial \gamma} \\ \frac{\partial^2 m}{\partial \beta \cdot \partial \alpha} & \frac{\partial^2 m}{\partial \beta \cdot \partial \beta} & \frac{\partial^2 m}{\partial \beta \cdot \partial \gamma} \\ \frac{\partial^2 m}{\partial \gamma \cdot \partial \alpha} & \frac{\partial^2 m}{\partial \gamma \cdot \partial \beta} & \frac{\partial^2 m}{\partial \gamma \cdot \partial \gamma} \end{bmatrix} \quad (m = l_{01}, l_{02}, l_{03}) \quad (61)$$

IV. STIFFNESS ANALYSIS

When loads are applied to the robot, its end effector produces undesirable displacement, which directly affects the robot's position accuracy. Since the robot's accuracy is mainly affected by the stiffness, it would be important to analyze the stiffness. In particular, the relationship between the driving system's stiffness and the end effector's stiffness should be clarified. It is worth mentioning that, to simplify the modeling, driven system is regarded as a flexible part, while the others as rigid ones.

Representing the force vector of the driving joint in the three limbs with $\mathbf{f} = [f_1 f_2 f_3]^T$, the corresponding deformation with $\Delta \mathbf{q} = [\Delta q_1 \Delta q_2 \Delta q_3]^T$, and the stiffness coefficient with $\mathbf{k} = \text{diag}(k_1, k_2, k_3)$, respectively, we have

$$\mathbf{f} = \mathbf{k} \Delta \mathbf{q} \quad (62)$$

Meanwhile, the force vector of the leg-end is $\mathbf{F} = [F_1 F_2 F_3]^T$, and corresponding deformation is $\Delta \mathbf{Q} = [\Delta Q_1 \Delta Q_2 \Delta Q_3]^T$, and \mathbf{K} is the stiffness Jacobian matrix, then their relationship is that

$$\mathbf{F} = \mathbf{K} \Delta \mathbf{Q} \quad (63)$$

By rewriting the Jacobian matrix into the differential form:

$$\Delta \mathbf{q} = \mathbf{J} \Delta \mathbf{Q} \quad (64)$$

According to the principle of virtual work, we obtain that,

$$\begin{cases} \mathbf{f}^T \Delta \mathbf{q} = \sum_{i=1}^3 f_i^T \Delta q_i \\ \mathbf{F}^T \Delta \mathbf{Q} = \sum_{i=1}^3 F_i^T \Delta Q_i \\ \mathbf{f}^T \Delta \mathbf{q} = \mathbf{F}^T \Delta \mathbf{Q} \end{cases} \quad (65)$$

Substituting (62), (63) and (64) into (65), we obtain that

$$\mathbf{K} = \mathbf{J}^T \mathbf{k} \mathbf{J} \quad (66)$$

There are many methods for evaluating the stiffness of a mechanism, e.g., the determinant, the condition number, as well as the eigenvalue distribution of the stiffness

Jacobian matrix. To clearly show the influence of the stiffness of driving joints and the error of the Jacobian matrix on the stiffness Jacobian matrix of the leg-end, we use the condition number of the stiffness Jacobian matrix to evaluate the stiffness of this mechanism. The results obtained by numerical analysis are shown in Fig. 5. In the workspace, the condition numbers of stiffness Jacobian matrix at $z = 500, 600, 700$, and 800 mm are shown in Figs. 5(a), (b), (c), and (d), respectively.

As shown in Fig. 5, the condition number of the stiffness Jacobian matrix is satisfactorily small in the whole working space; this indicates that the robot is capable of obtaining high stiffness and avoiding large force error of the leg-end induced by the errors of the joints' force and Jacobian matrix.

V. SIMULATION ANALYSIS

To verify the effectiveness of the above analysis, a simulation is implemented. First, the mechanism is modeled with SolidWorks (ver. 2016). Then, the model, where constraints and actuating conditions are considered, is analyzed with ADMAS (ver. 2013). Finally, the simulated results are compared with the theoretical values.

Prior to simulation, the initial position of point P is set at $[-400 \ 0 \ -450]^T$ and three electric push rods' velocities are expressed as

$$\begin{cases} v_1 = 20 \sin t \\ v_2 = 20 \sin t \\ v_3 = 20 \sin t \end{cases} \quad (67)$$

The displacements of the three rods are given as

$$\begin{cases} d_1 = -20 \cos t + 20 \\ d_2 = -20 \cos t + 20 \\ d_3 = -20 \cos t + 20. \end{cases} \quad (68)$$

Using MATLAB (ver. R2014a), the results obtained through theoretical analysis and simulation are processed. The displacement, velocity and acceleration of point P are shown in Figs. 6, 7, and 8, respectively. It can be observed that the theoretical values (indicated in black lines) agree with the simulated results (red lines); this shows that the theoretical analysis is effective.

VI. EXPERIMENT

A prototype of the (2-UPS+U)&(R+RPS) mechanism was fabricated. The photo of the prototype is shown in Fig. 9. The prototype consists of a frame, an upper leg, a lower leg, three electric push rods (SC0, Shidaichaoqun Corp., Beijing, China), a wheel, and a controller. The upper and lower legs are 450 and 400 mm, respectively.

To evaluate the accuracy, it is necessary to measure the position error. Currently, commonly used calibration methods include direct and indirect approaches. The direct method tracks the positions of the reference point of the measured object, while the indirect method calculates the parameter

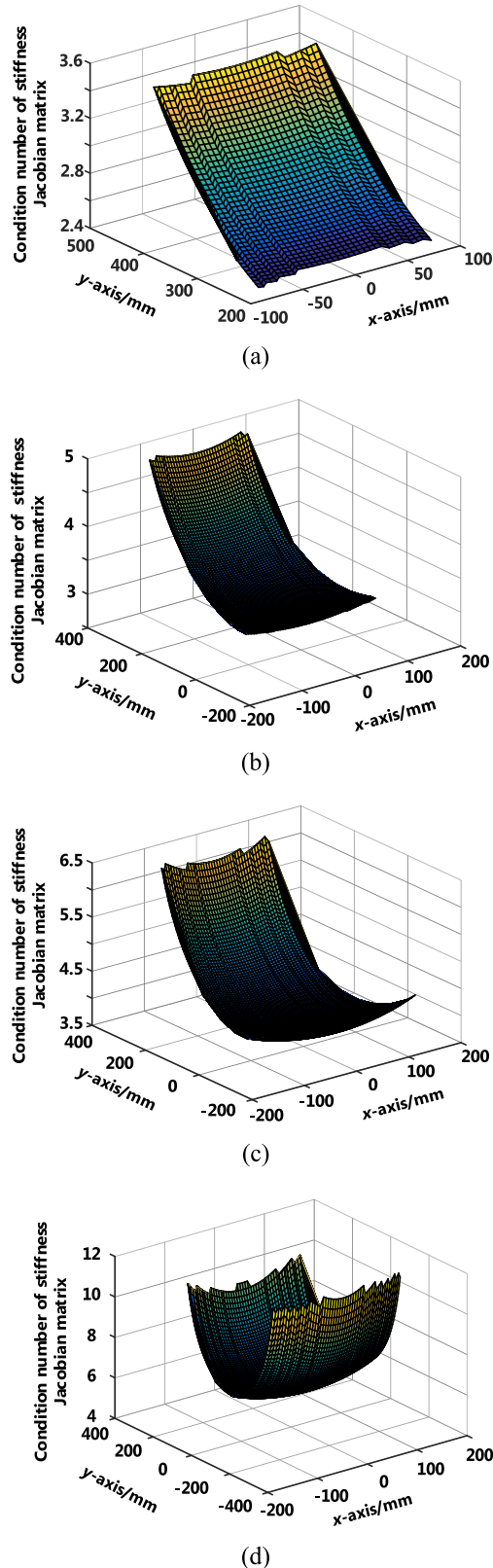


FIGURE 5. Distribution of the condition number of stiffness Jacobian matrix in workspace. (a) $z = 500$, (b) $z = 600$, (c) $z = 700$, and (d) $z = 800$ mm.

changes, as measured with length/angle sensors, through forward kinematics [35]. In comparison, the results obtained by

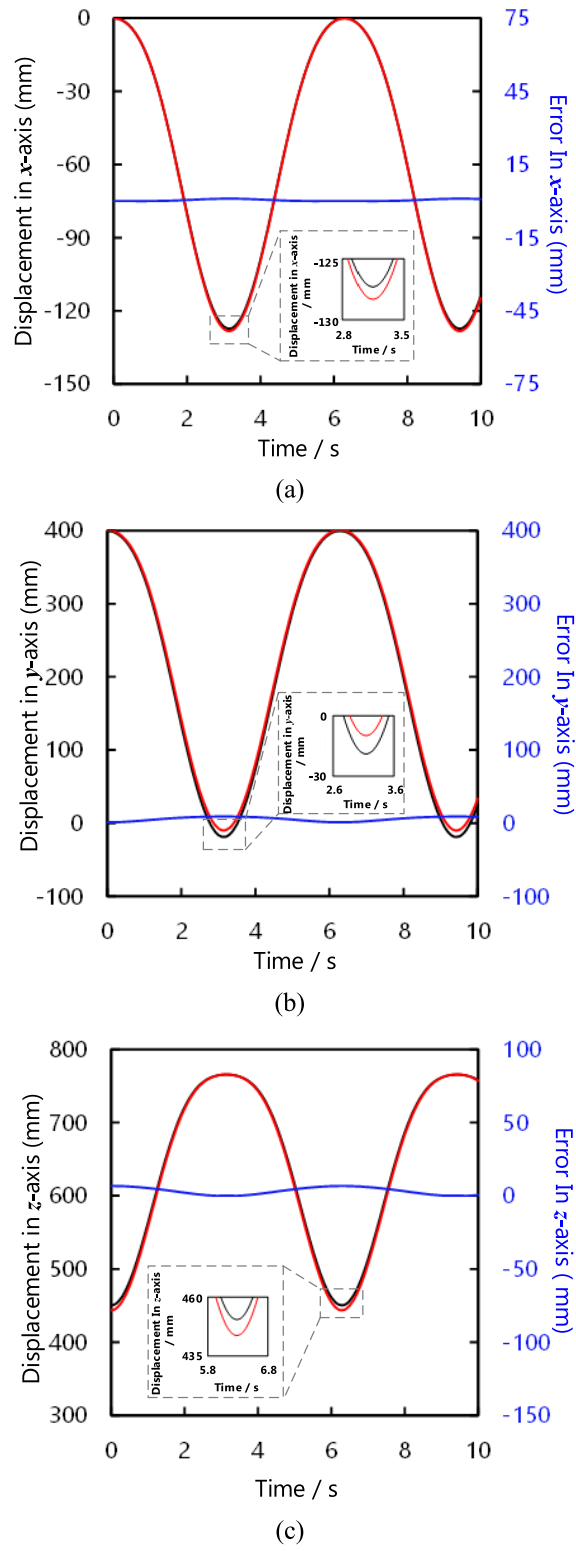


FIGURE 6. Comparison between the calculated and simulated values of the displacements in (a) x -, (b) y -, and (c) z -axes.

the direct method include the assembly errors and control errors of each limb, and the overall accuracy is theoretically higher than the indirect method; thus, the direct method is selected.

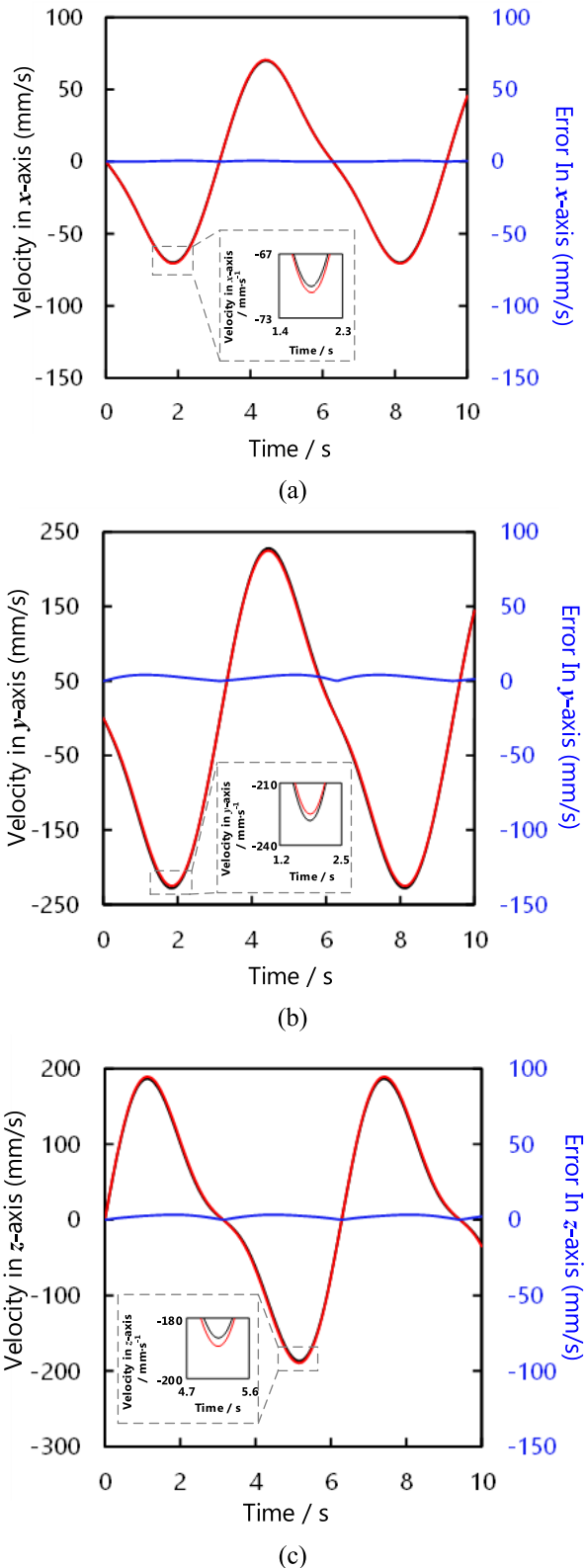


FIGURE 7. Comparison between the calculated and simulated values of the velocities in (a) x-, (b) y-, and (c) z-axes.

The instrument used in the experiment was a Vicon MX motion capture system (OML Corp., Oxford, UK). Four cameras tracked the markers in real time. The experimental setup

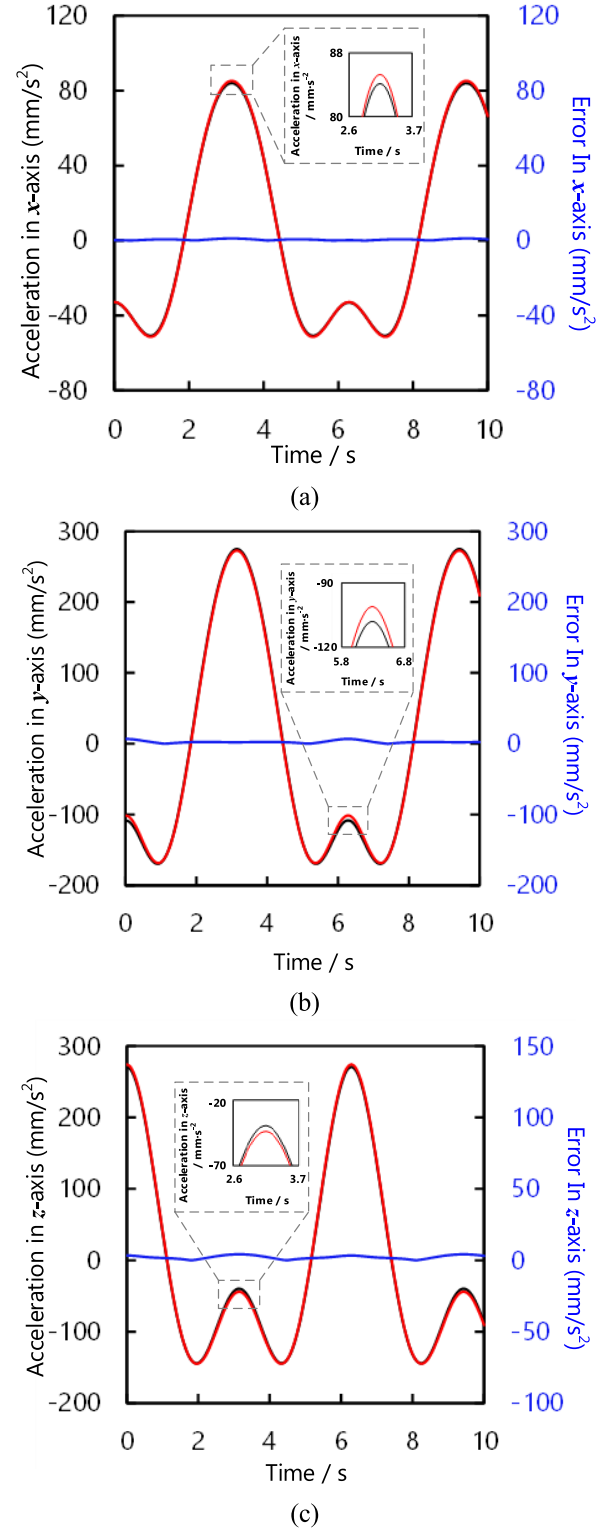


FIGURE 8. Comparison between the calculated and simulated values of the accelerations in (a) x-, (b) y-, and (c) z-axes.

is shown in Fig. 10. The experimental processes are listed as follows:

- (1) The prototype was fixed to the calibration stand, and reflective balls, used as markers, were bonded to

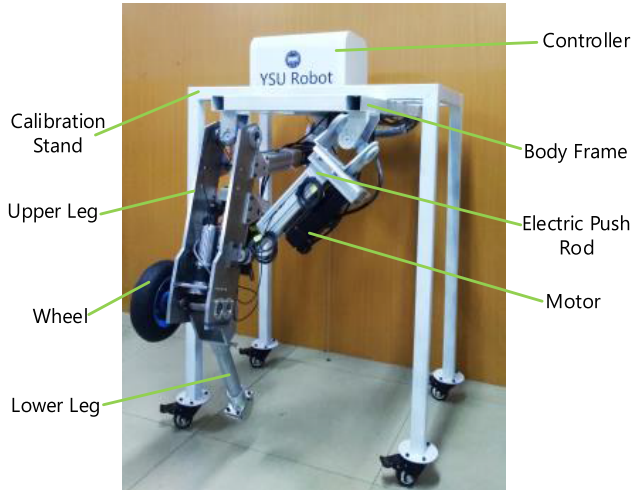


FIGURE 9. Photo of the (2-UPS+U)&(R+RPS) mechanism prototype.

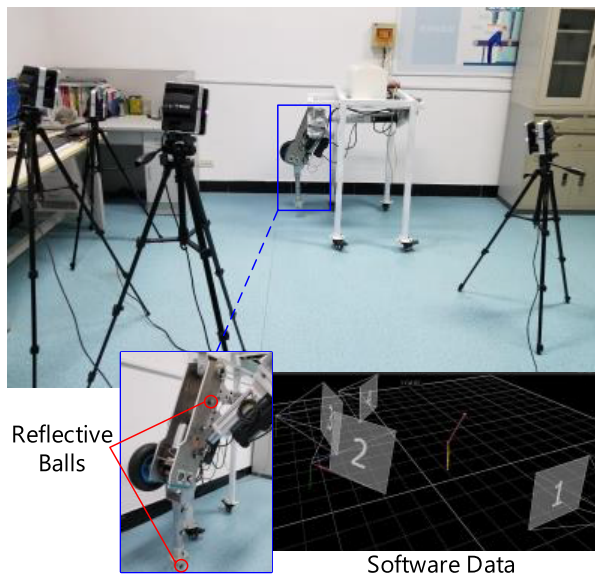


FIGURE 10. Calibration experiment.

the prototype. The position of the prototype was adjusted to ensure that the position of each ball could be captured with three cameras.

(2) The origin of the spatial coordinate system was determined with a T-shaped calibration frame.

(3) A trajectory was planned and the electric push rods were actuated to enable the movement of the prototype to fit the trajectory. The cameras were used to record the real positions of the mechanism. The experiments were carried out 5 times.

(4) The positions obtained from the 5 experimental runs were averaged as the trajectory curve and the error of each point was obtained by comparing them with the planned curve.

The planned trajectory curve and the experimental trajectory of point P is shown in Fig. 11. The maximum deviation in the y-axis displacement between the actual and planned

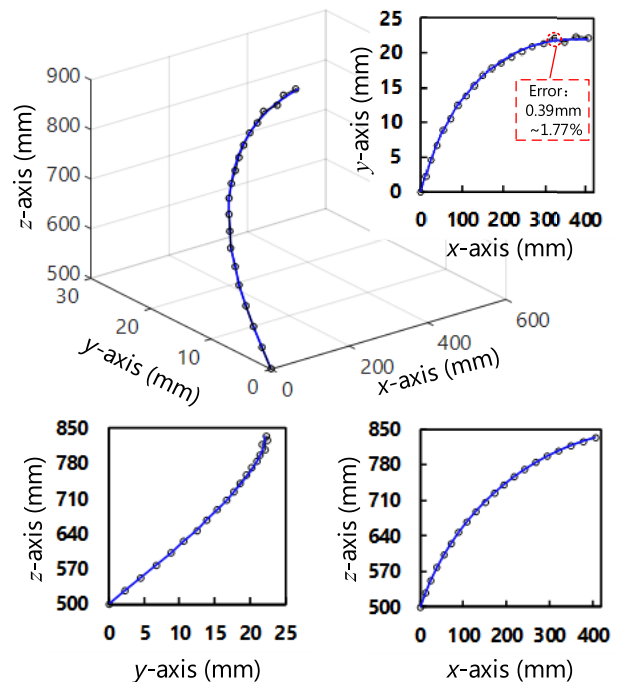


FIGURE 11. Experimental results and the planned trajectory curve (indicated as dots and the curve, respectively).

TABLE 2. Comparison in stiffness and accuracy between previously-reported and current mechanisms.

Indicator	Current mechanism	The mechanism reported in ref. [29]
Stiffness (N/m)	Maximal eigenvalue	5.43×10^5
	Minimal eigenvalue	5.69×10^4
Accuracy	Δx_{\max}	0.9%
	Δy_{\max}	1.8%
	Δz_{\max}	1.1%

curves was 0.39 mm, corresponding to a maximum error of 1.8%. The spatial curve was entirely smooth, particularly in the xz plane; this implied that the robot could move smoothly when the robot walked forward. Because the movement of the prototype in the y direction was not sufficiently stable, the trajectories in the xoy and yoz planes were not smooth. In particular, the curves oscillated in the y range between 20 and 22 mm. This result was likely caused by jitter when the electric push rod reached the end.

In addition, the mechanism could move smoothly in the x -axis range of >400 mm and the z -axis range of >300 mm, both of which implied its suitability as the leg of a wheel-legged robot.

Finally, the stiffness and position accuracy of the current mechanism are compared with those of the mechanism reported in [29]. Observably, the stiffness is approximately twice higher for the current than for the previously-reported mechanism. On the other hand, the z -axis accuracy of the

current mechanism is 4% higher than that of the previous one. These results prove the advantages of the current mechanism, i.e., high stiffness and high accuracy, as shown in Table 2.

VII. CONCLUSION

In this paper, a 3-DOF serial-parallel mechanism is proposed, and its feasibility and potential are proved through theoretical analyses and experiments. First, by analyzing the mobility of the mechanism, the configuration has 3 DOFs, which include rotations around the x -, y - and x_k -axes. Then, kinematics analyses and simulations are conducted, and the results well agree with the theoretical values; this indicates that the theoretical derivations of the position, Jacobian matrix, velocity, acceleration, and inverse kinematics of the mechanism are effective. Finally, the mechanism prototype is fabricated, and its performance is evaluated. The experiments show that the mechanism offers high motion accuracy and a large workspace, both of which imply its suitability as a leg for wheel-legged robots.

In this study, the kinematic properties of our mechanism are systematically studied, and most of them are clarified. However, since only one leg has been made up to the present, the bearing capability of the mechanism has not been verified; this problem is left for further work. On the other hand, other kinematic properties, i.e., dexterity and singularity, will be explored. In addition, we will apply the mechanism to a robot and assess its dynamic characteristics, gait planning, and control method, all of which are necessary aspects in practical robot applications and are worth investigating in future work.

REFERENCES

- [1] A. Suzumura and Y. Fujimoto, "Real-time motion generation and control systems for high wheel-legged robot mobility," *IEEE Trans. Ind. Electron.*, vol. 61, no. 7, pp. 3648–3659, Jul. 2014.
- [2] M. Bjelonic, C. D. Bellicoso, Y. Viragh, D. Sako, F. D. Tresoldi, F. Jenelten, and M. Hutter, "Keep rollin'—Whole-body motion control and planning for wheeled quadrupedal robots," *IEEE Robot. Automat. Lett.*, vol. 4, no. 2, pp. 2116–2123, Apr. 2019.
- [3] B. H. Wilcox, "ATHLETE: A mobility and manipulation system for the moon," in *Proc. IEEE Aerosp. Conf.*, Big Sky, MT, USA, Mar. 2007, pp. 1–10.
- [4] S. Hirose and H. Takeuchi, "Study on roller-walk (basic characteristics and its control)," in *Proc. IEEE Int. Conf. Robot. Autom.*, Minneapolis, MN, USA, Apr. 1996, pp. 3265–3270.
- [5] S. Fujii, K. Inoue, T. Takubo, and T. Arai, "Climbing up onto steps for limb mechanism robot, 'ASTERISK,'" in *Proc. 23rd Int. Symp. Rob. Autom. Const.*, Tokyo, Japan, 2006, pp. 225–230.
- [6] G. Besseron, C. Grand, F. Ben Amar, and P. Bidaud, "Decoupled control of the high mobility robot hylos based on a dynamic stability margin," in *Proc. IEEE/RSJ Int. Conf. Intell. Robots Syst.*, Nice, France, Sep. 2008, pp. 2435–2440.
- [7] A. Gronowicz, P. Sperzyński, J. Szrek, and J. Jakubiak, "Wheel-legged robot-construction and obstacle detection sensors," *Mech. Mach. Sci.*, vol. 17, pp. 191–198, Jan. 2014.
- [8] B. Huang, P. Wang, and L. Sun, "Behavior-based control of a hybrid quadruped robot," in *Proc. 6th World Congr. Intell. Control Autom.*, Dalian, China, Jun. 2006, pp. 8997–9001.
- [9] W. Shen, Z. Pan, M. Li, and H. Peng, "A lateral control method for wheel-footed robot based on sliding mode control and steering prediction," *IEEE Access*, vol. 6, pp. 58086–58095, 2018.
- [10] A. Halme, I. Leppänen, J. Suomela, S. Ylönen, and I. Kettunen, "Work-Partner: Interactive human-like service robot for outdoor applications," *Int. J. Robot. Res.*, vol. 22, nos. 7–8, pp. 627–640, Jul. 2003.
- [11] J. Muller, M. Schneider, and M. Hiller, "Modeling, simulation, and model-based control of the walking machine ALDURU," *IEEE/ASME Trans. Mechatronics*, vol. 5, no. 2, pp. 142–152, Jun. 2000.
- [12] J. A. Smith, I. Sharf, and M. Trentini, "PAW: A hybrid wheeled-leg robot," in *Proc. IEEE Int. Conf. Robot. Autom. (ICRA)*, Orlando, FL, USA, May 2006, pp. 4043–4048.
- [13] Q. Chang, X. Liu, W. Xu, L. Yan, and B. Yang, "The design and experiments of a small wheel-legged mobile robot system with two robotic arms," in *Proc. IEEE/RSJ Int. Conf. Intell. Robots Syst. (IROS)*, Daejeon, South Korea, Oct. 2016, pp. 2590–2595.
- [14] S. Dubey, M. Prateek, and M. Saxena, "Robot locomotion-a review," *Int. J. Appl. Eng. Res.*, vol. 10, no. 3, pp. 7357–7369, 2015.
- [15] Z. Wang, X. Ding, Y. Xie, A. Rovetta, C. Paul, and D. I. Espinosa, "Conceptual design of a novel robotics system for planetary exploration," in *Proc. 6th World Congr. Intell. Control Autom.*, Dalian, China, 2006, pp. 8962–8965.
- [16] Boston Dynamics. *Handle Mobile Box Handling Robots for Logistics*. Accessed: Apr. 19, 2019. [Online]. Available: <https://www.bostondynamics.com/handle>
- [17] M. Lacagnina, G. Muscato, and R. Sinatra, "Kinematics, dynamics and control of a hybrid robot wheeleg," *Robot. Auto. Syst.*, vol. 45, nos. 3–4, pp. 161–180, Dec. 2003.
- [18] Y. Xin, H. Chai, Y. Li, X. Rong, B. Li, and Y. Li, "Speed and acceleration control for a two wheel-leg robot based on distributed dynamic model and whole-body control," *IEEE Access*, vol. 7, pp. 180630–180639, 2019.
- [19] G. S. Thornton, "The GEC Tetrabot—a new serial-parallel assembly robot," in *Proc. IEEE Int. Conf. Robot. Automat.*, Philadelphia, PA, USA, Apr. 1988, pp. 437–439.
- [20] C. Giuseppe and C. Marco, "A serial-parallel robotic architecture for surgical tasks," *Robotica*, vol. 23, no. 3, pp. 345–354, May/Jun. 2005.
- [21] S.-H. Cha, T. Lasky, and S. Velinsky, "Kinematic redundancy resolution for serial-parallel manipulators via local optimization including joint constraints," *Mech. Based Des. Struct. Mach.*, vol. 34, no. 2, pp. 213–239, 2006.
- [22] J. Gao, Y. Wang, Q. Yu, and W. Zuo, "Study on gait planning and simulation of a novel hybrid quadruped robot," *Mech. Mach. Sci.*, vol. 55, pp. 1225–1239, 2018.
- [23] C. Hou, P. Zhang, Y. Hu, and J. Zhang, "The dynamics analysis for a five DOF serial-parallel manipulator with RP-(2-RRU/1-RUU) structure," in *Proc. IEEE Int. Conf. Robot. Biomimetics (ROBIO)*, Guangzhou, China, Dec. 2012, pp. 1564–1569.
- [24] A. Peidró, A. Gil, J. M. Marín, Y. Berenguer, and L. Payá, "Monte-Carlo workspace calculation of a serial-parallel biped robot," in *Proc. 2nd Iber. Rob. Conf., Adv. Robot.*, Lisbon, Portugal, 2015, pp. 57–169.
- [25] D. Zhang and Z. Gao, "Optimal kinematic calibration of parallel manipulators with pseudoerror theory and cooperative coevolutionary network," *IEEE Trans. Ind. Electron.*, vol. 59, no. 8, pp. 3221–3231, Aug. 2012.
- [26] Y. Lu, Z. Dai, N. Ye, and P. Wang, "Kinematics/statics analysis of a novel serial-parallel robotic arm with hand," *J. Mech. Sci. Technol.*, vol. 29, no. 10, pp. 4407–4416, Oct. 2015.
- [27] X. Wang, Z. Jin, and X. Li, "Analysis of static performance of serial-parallel hybrid bionic mechanical leg," *Trans. Chin. Soc. Agricult. Mach.*, vol. 50, no. 1, pp. 383–389, Jan. 2019.
- [28] Z. Gao and D. Zhang, "Performance analysis, mapping, and multiobjective optimization of a hybrid robotic machine tool," *IEEE Trans. Ind. Electron.*, vol. 62, no. 1, pp. 423–433, Jan. 2015.
- [29] J. Niu, H. Wang, H. Shi, N. Pop, D. Li, and W. Wu, "Study on structural modeling and kinematics analysis of a novel wheel-legged rescue robot," *Int. J. Adv. Robotic Syst.*, vol. 15, no. 1, Jan. 2018, Art. no. 1729881417752758.
- [30] Z. Huang, Y. Zhao, and T. Zhao, *Advanced Spatial Mechanism*, 2nd ed. Beijing, China: Higher Education Press, 2014, pp. 111–155.
- [31] J. Zhang, Z. Jin, and H. Feng, "Type synthesis of a 3-mixed-DOF protectable leg mechanism of a firefighting multi-legged robot based on GF set theory," *Mechanism Mach. Theory*, vol. 130, pp. 567–584, Dec. 2018.
- [32] D. Zhang, Y. Xu, J. Yao, B. Hu, and Y. Zhao, "Kinematics, dynamics and stiffness analysis of a novel 3-DOF kinematically/actuation redundant planar parallel mechanism," *Mechanism Mach. Theory*, vol. 116, pp. 203–219, Oct. 2017.
- [33] B. Han, D. Zheng, Y. Xu, J. Yao, and Y. Zhao, "Kinematic characteristics and dynamics analysis of an overconstrained scissors double-hoop truss deployable antenna mechanism based on screw theory," *IEEE Access*, vol. 7, pp. 140755–140768, 2019.

- [34] B. Hu, J. Zhao, and H. Cui, "Terminal constraint and mobility analysis of serial-parallel manipulators formed by 3-RPS and 3-SPR PMs," *Mechanism Mach. Theory*, vol. 134, pp. 685–703, Apr. 2019.
- [35] L. Fan, A. Y. Elatta, and X. Li, "Kinematic calibration for a hybrid 5DOF manipulator based on 3-RPS in-actuated parallel manipulator," *Int. J. Adv. Manuf. Technol.*, vol. 25, nos. 7–8, pp. 730–734, Apr. 2005.



JIANYE NIU received the B.S. degree in mechanical engineering, and the M.S. and Ph.D. degrees in mechatronic engineering from Yanshan University, Qinhuangdao, China, in 2005, 2008, and 2019, respectively.

He is currently a Postdoctoral Researcher with the School of Mechanical Engineering, Hebei University of Technology, Tianjin, China. His research interests include parallel mechanism and its application, rehabilitation robot, mechanical engineering, and artificial neural networks.



HONGBO WANG (Member, IEEE) received the B.S. and M.S. degrees from the Institute of Northeast Heavy Machinery, Qiqihar, China, in 1982 and 1986, respectively, and the Ph.D. degree from Nagasaki University, Nagasaki, Japan, in 1997.

From 1992 to 1993, he was a Visiting Scholar with the Institute of Robotics, ETH Zuerich, Switzerland. He was a Researcher with Nagasaki University. Since 2009, he has been working as

a Professor with Yanshan University, Qinhuangdao, China. His current research interests include rehabilitation robot and assisting robot for the disabled and the elderly.



ZHIWEN JIANG was born in Yichang, Hubei, China, in 1995. He received the B.S. degree in mechanical design, manufacturing and automation from the Hebei University of Technology, Tianjin, China, in 2017, where he is currently pursuing the M.S. degree in mechanical engineering.

His research interests include dynamic model applied to nursing robot, rehabilitation robot, and wearable exoskeleton.



LI CHEN was born in Longyan, Fujian, China, in 1991. He received the B.S. degree in mechanical design, manufacturing and automation from the Harbin Institute of Technology, Harbin, China, in 2014. He is currently pursuing the M.S. degree in mechanical engineering with the Hebei University of Technology, Tianjin, China.

His research interests include robot manipulator control and motion planning.



design theory of parallel robot.

JIANJUN ZHANG received the Dr.Eng. degree in mechanical engineering from Beihang University, in 2004.

From 2006 to 2008, he was a Visiting Scholar with the Harbin Institute of Technology, Shenzhen. He is currently a Professor with the School of Mechanical Engineering, Hebei University of Technology, Tianjin, China. He has authored or coauthored over 50 peer-reviewed articles. His research interests include mechanism of robot and



YONGFEI FENG received the B.S. degree in mechanical engineering and the Ph.D. degree in mechatronic engineering from Yanshan University, Qinhuangdao, China, in 2012 and 2018, respectively.

He was once a joint doctoral-student with Yan-shan University, China. From September 2016 to October 2017, he was with the Institute of Solid Mechanics of Romanian Academy, Romania. He is currently a Lecturer with Ningbo University, Ningbo, China. His research interests include parallel mechanism and its application, rehabilitation robot, mechanical engineering, and artificial neural networks.



SHIJIE GUO (Member, IEEE) received the Dr.Eng. degree in mechanical engineering from the Tokyo Institute of Technology, in 1992.

He was the Team Leader of the Robot Implementation Research Team, RIKEN-TRI Collaboration Center for Human-Interactive Robot Research, RIKEN. From August 2007 to March 2015, he was the Head of the Healthcare Division of Sumitomo Riko Ltd., Japan. He is currently a Professor with the School of Mechanical Engineering, Hebei University of Technology, Tianjin, China. He is also the Head of the Hebei Key Laboratory of Robot Perception and Human-robot Interaction, Hebei University of Technology. He is also a Professor with the Institute of AI and Robotics, Fudan University and the Principal Scientist with the State Key Laboratory for Reliability and Intelligence of Electrical Equipment. His current research interests include nursing-care systems, including transfer assistant robots, walking assist robots, smart care beds, and unconstrained measurement of vital information. His is a member of JSME. He is the Editor-in-Chief of the *Journal of Hebei University of Technology*.